Influence of Hydrophobicity on the Surface-Catalyzed Assembly of the Islet Amyloid Polypeptide

Adrian Keller,[†,*] Monika Fritzsche,[‡] Ye-Ping Yu,[§] Qian Liu,[§] Yan-Mei Li,[§] Mingdong Dong,[†] and Flemming Besenbacher[†,⊥]

[†]Interdisciplinary Nanoscience Center (iNANO), Aarhus University, Ny Munkegade, 8000 Aarhus C, Denmark, [‡]Institute of Ion Beam Physics and Materials Research, Helmholtz-Zentrum Dresden-Rossendorf, PO Box 510119, 01314 Dresden, Germany, [§]Key Lab of Bioorganic Phosphorus Chemistry & Chemical Biology, Department of Chemistry, Tsinghua University, Beijing 100084, People's Republic of China, and [⊥]Department of Physics and Astronomy, Aarhus University, 8000 Aarhus C, Denmark

ABSTRACT The islet amyloid polypeptide (IAPP) is a hormonal factor secreted by the β-cells in the pancreas. Aggregation of misfolded IAPP molecules and subsequent assembly of amyloid nanofibrils are critical for the development of type 2 diabetes mellitus. In the physiological environment, amyloid aggregation is affected by the presence of interfaces such as cell membranes. The physicochemical properties of the interface dictates the interaction of the peptide with the surface, *i.e.*, electrostatic and hydrophobic interactions on hydrophilic and hydrophobic surfaces, respectively. We have studied the influence of hydrophobicity on the surface-catalyzed assembly of IAPP on ultrasmooth hydrocarbon films grown on ion-beam-modified mica surfaces by atomic force microscopy. The contact angle θ of these surfaces can be tuned continuously in the range from $\leq 20°$ to $\sim 90°$ by aging the samples without significant changes of the chemical composition or the topography of the surface. On hydrophilic surfaces with a θ of $\sim 20°$, electrostatic interactions induce the assembly of IAPP nanofibrils, whereas aggregation of large ($\sim$2.6 nm) oligomers is observed at hydrophobic surfaces with a θ of $\sim 90°$. At intermediate contact angles, the interplay between electrostatic and hydrophobic substrate interactions dictates the pathway of aggregation with fibrillation getting continuously delayed when the contact angle is increased. In addition, the morphology of the formed protofibrils and mature fibrils at intermediate contact angles differs from those observed at more hydrophilic surfaces. These results might contribute to the understanding of the surface-catalyzed assembly of different amyloid aggregates and may also have implications for the technologically relevant controlled synthesis of amyloid nanofibrils of desired morphology.

KEYWORDS: amyloid · IAPP · hydrophobicity · atomic force microscopy · mica · ion-beam modification

Protein denaturation and amyloid aggregation play important roles in the development of so-called protein-misfolding diseases such as Alzheimer's disease, Parkinson's disease, and type 2 diabetes mellitus.[1] In the course of these diseases, partially unfolded proteins associate with one another and form oligomeric structures of up to several nanometers in diameter.[2] These oligomers then can further assemble into protofibrils and finally mature fibrils consisting of coiled protofibrils.[3,4] Many different factors may act as the initial trigger of the protein misfolding and subsequent aggregation, including pH, ionic strength, and protein concentration.

In the physiological environment, many processes are dictated by interfacial phenomena. In the case of amyloid aggregation, the presence of a surface may induce the formation of initial oligomers and influence the assembly rate and the structure of the aggregates. Thus, numerous *in vitro* studies have investigated amyloid aggregation and fibrillation on various model surfaces in order to identify the influence of the physicochemical surface properties on the aggregation.[5−24] The model surfaces used in these studies included (chemically modified) mica,[6−9,12,18] highly oriented pyrolytic graphite (HOPG),[7,12,16] silica,[13,14,21] different polymers,[5,11,14,15,20−24] and lipid films.[10,17,19] Indeed, these studies showed that the surface has a strong effect on the amyloid aggregation. Insulin aggregation on hydrophobic Teflon surfaces was found to proceed at a higher rate than in the bulk.[5] The same surface also induced conformational changes in aggregates of the Alzheimer β-amyloid compared to those formed in solution.[11] Similarly, the islet amyloid polypeptide was observed to form fewer higher order fibrils on hydrophilic mica surfaces than in the bulk.[6]

In order to understand how the physicochemical properties of different surfaces influence the amyloid aggregation, model surfaces with tailored properties are needed. However, it remains a challenge to create model surfaces that allow for the fine-tuning of certain physicochemical properties without affecting others. This is particularly true for the hydrophobicity of the surface. In the past, the influence of hydrophobicity on amyloid aggregation

* Address correspondence to adrian@inano.au.dk.

Received for review November 24, 2010 and accepted March 24, 2011.

Published online March 31, 2011
10.1021/nn1031998

and fibrillation has been assessed by comparing physically and chemically different model surfaces of hydrophilic and hydrophobic nature such as mica vs HOPG,[7,12] Teflon vs silica,[14] or different polymers.[15,20,22] Kowalewski and Holtzman investigated the assembly of the amyloid β-peptide on hydrophilic mica and hydrophobic HOPG.[7] On mica, they observed oligomeric and protofibrillar aggregates, whereas elongated β-sheets following certain crystallographic directions of the surface were found on HOPG. Similar β-sheet lamellae on HOPG have also been observed for other amyloid-forming peptides.[25,26] In contrast to these observations, Hoyer *et al*. found ordered β-sheet lamellae of α-synuclein, a protein related to Parkinson's disease, on mica surfaces with their orientation dictated by the crystallinity of the surface.[12] On HOPG, however, the lamellae formation was suppressed for this protein. This demonstrates how strongly the assembly of different amyloid-forming peptides and proteins is influenced by the structure of the model surface.

Nayak *et al*. studied the interaction of insulin with different polymer membranes and concluded that smooth hydrophilic surfaces tend to inhibit insulin fibrillation.[20] However, Jeworrek *et al*. observed the strongest insulin adsorption on a hydrophilic, negatively charged poly(styrene sulfonate) surface compared to a hydrophobic polystyrene surface.[22] This shows that also when comparing noncrystalline hydrophilic and hydrophobic model surfaces, other surface properties such as the chemical composition, surface charge, and surface roughness play an important role. Especially the surface roughness has a strong effect on the adsorption of proteins[27] and is usually hard to control.[20] In order to minimize the undesired effects of different chemical composition and surface roughness, we have utilized a novel type of model surface to study amyloid assembly on surfaces with different wettability. For this, ultrathin hydrocarbon (HC) films of a few monolayers thickness have been grown on atomically flat ion-beam-modified mica surfaces. Low-energy ion-beam processing is a common technique frequently used to modify the physicochemical properties of mica surfaces for various applications such as organic thin film growth.[28] The contact angle of the so-produced negatively charged mica/HC surfaces can be tuned continuously in the range from <20° to ~90° without significant changes in the roughness or the chemical composition of the film surface.[29]

By using mica/HC surfaces with different contact angles, the influence of hydrophobicity on the surface-catalyzed assembly of the islet amyloid polypeptide (IAPP) at the solid−liquid interface is investigated in detail. IAPP is a hormone co-secreted with insulin by the β-cells in the pancreas. The 37-amino-acid residue peptide represents the main component of the amyloid deposits found in the islets of Langerhans of type 2 diabetes patients.[3] Both the oligomeric[30] and the fibrillar species[31] of the IAPP amyloid have been found to damage membranes and can thus induce apoptosis of the insulin-producing β-cells.[32] Our investigation reveals a strong dependence of the interface-induced IAPP aggregation and fibrillation on the hydrophobicity of the surface. In particular, the hydrophobicity of the surface dictates the type of aggregates, *i.e*., oligomers and fibrillar structures of different size and morphology. These observations can be explained as resulting from the interplay between electrostatic and hydrophobic interactions with the surface.

These results could be beneficial for the understanding of the surface-catalyzed amyloid assembly and inspire novel routes for the technologically relevant controlled synthesis of certain types of nanofibrils of desired morphology.[33]

RESULTS

Figure 1 shows atomic force microscopy (AFM) images of the IAPP aggregation on the mica/HC surface with a contact angle θ of ~23°. After 30 min of incubation (Figure 1a,b), a thin film is found on the surface. The film is not closed yet and consists of connected fractal-shaped islands. The high-resolution AFM image shown in Figure 1b reveals the presence of smaller islands of lower height between the larger, fractal ones. The height of these islands is about 0.4 nm, whereas the larger fractal islands have a height of about 0.8 nm. This indicates that the film consists of mono- and bilayers of adsorbed IAPP monomers and thus represents the earliest stage of the IAPP interaction with the surface. However, as can be seen in Figure 1b, also a few larger, particle-like structures are present. These particles have heights ranging from ~0.3 to ~2.5 nm, indicating that the particles represent different species of oligomers. The main species has a height of 0.7 ± 0.2 nm. Figure 1b1 depicts height profiles of two different oligomers taken between the arrows indicated in Figure 1b.

After 1 h of incubation (Figure 1c,d), the monomer film is more or less closed and many protofibrils of various lengths have assembled on the surface. Furthermore, rather large, amorphous deposits are found. As the high-resolution image in Figure 1d shows, also the protofibrils are decorated with amorphous aggregates and possibly also oligomeric structures. The protofibrils have a height of 2.0 ± 0.5 nm.

The first higher-order fibrils are observed after 2.5 h incubation time (Figure 1e,f). These mature fibrils have an increased height of 4.5 ± 0.5 nm, which is about twice the height of the protofibrils. In addition to the mature fibrils, there are still large numbers of protofibrils and oligomers present on the surface. This is demonstrated in Figure 1f1, which shows a height profile taken across a small oligomer (o), a protofibril

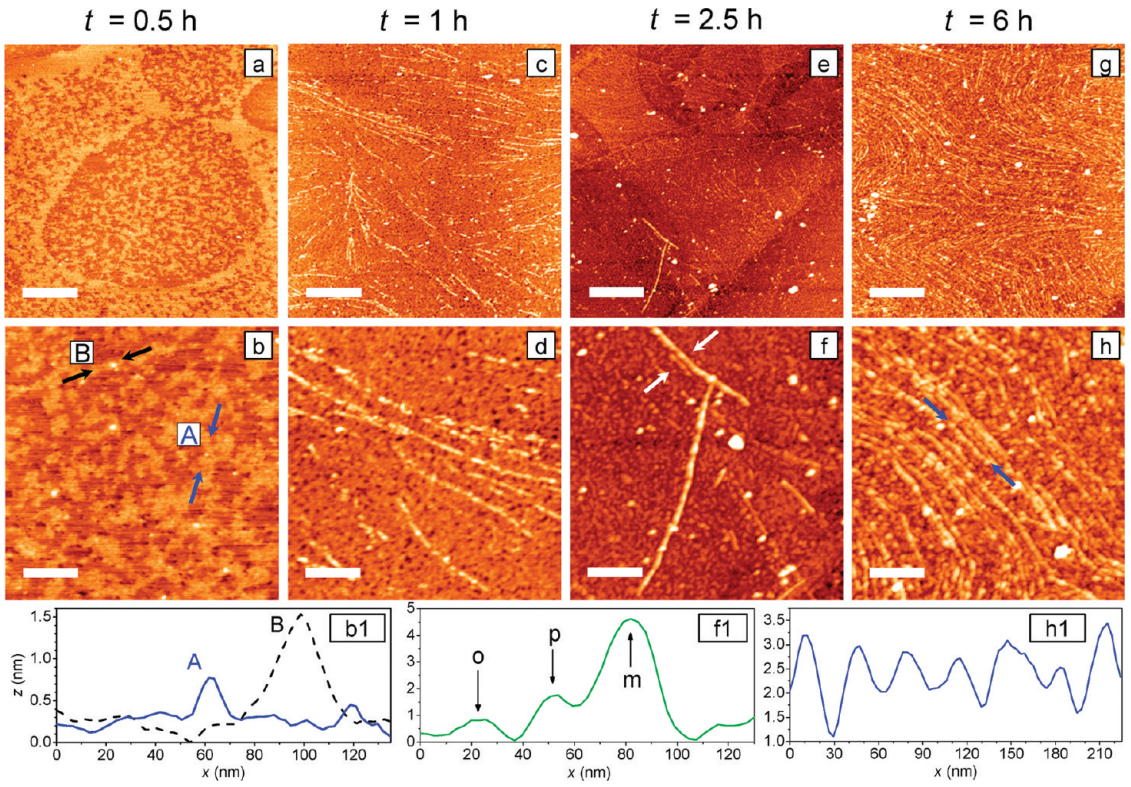

Figure 1. AFM images of the IAPP aggregation on a HC film with $\theta \approx 23°$ at $t = 0.5$ h (a, b), 1 h (c, d), 2.5 h (e, f), and 6 h (g, h). The scale bars are 660 (upper row) and 220 nm (center row); the height scales are 2 nm (a, b), 5 nm (c, d), and 8 nm (e−h). (b1), (f1), and (h1) give height profiles taken between the arrows shown in (b), (f), and (h), respectively. The arrows in (f1) indicate the positions of an oligomer (o), a protofibril (p), and a mature fibril (m).

(p), and a mature fibril (m). Furthermore, also the size and the density of the amorphous aggregates have increased.

Figure 1g,h shows the surface after 6 h of incubation. Now large areas of the surface are covered by a continuous film of amyloid deposits. These deposits consist mainly of mature fibrils and amorphous aggregates (cf. Figure 1h). Figure 1(h1) gives a height profile along one of the mature fibrils in Figure 1h. One can clearly see the periodic modulation resulting from the coiling of the protofibrils. The mean crossover repeat of the mature fibrils has been determined as 28.4 ± 3.7 nm.

On the surface with $\theta \approx 23°$, a high density of protofibrils has been observed already after 1 h of incubation (*cf.* Figure 1c,d). For an increased contact angle of $\theta \approx 38°$, however, no protofibrils are present after 1 h, as can be seen in Figure 2a,b. The only visible structures on this surface are amorphous aggregates and oligomers that seem to be adsorbed on top of a rather closed film of monomers (Figure 2b).

The first protofibrils on the $\theta \approx 38°$ surface are observed after 2.5 h of incubation, as is shown in Figure 2c,d. Similar to the $\theta \approx 23°$ case of Figure 1c,d, the protofibrils are decorated with amorphous aggregates and oligomers. After 6 h of incubation (Figure 2e,f), several long protofibrils are observed, accompanied by amorphous aggregates and oligomeric structures. Different types of oligomers are found, with the main species having a height of 1.3 ± 0.3 nm. The height of the protofibrils, however, is smaller than in the $\theta \approx 23°$ case with 0.9 ± 0.2 nm, which roughly corresponds to the height of the main oligomer species. The arrow in Figure 2f indicates a rare occasion where one can see a short region of a rather long fibril that has a larger height than the rest of the fibril. A closer inspection of the high-resolution image in Figure 2f suggests that a higher order fibril consisting of two coiled protofibrils is starting to form at this particular position. However, as is evident from the height profiles given in Figure 2(f1,f2), also the higher order fibril exhibits a different structure than on the more hydrophilic surface with a height of about 1.8 nm and a crossover repeat of about 20 nm.

A further increase of the contact angle to $\theta \approx 61°$ leads to a further delay of the onset of fibrillation. Figure 3a,b depicts this surface after 2.5 h incubation. Obviously, no fibrils as in the previous case with $\theta \approx 38°$ are observed. Instead, the larger oligomers with a height of ~1.3 nm are now the dominating species. Protofibrils start to form after about 4 h of incubation (Figure 3c,d), as do large amorphous aggregates. Even after 6 h of incubation (Figure 3e,f), only a few and rather short protofibrils are observed, which are of the same height as for $\theta \approx 38°$, *i.e.*, ~0.9 nm. No higher order fibrils are found on the surface, and large,

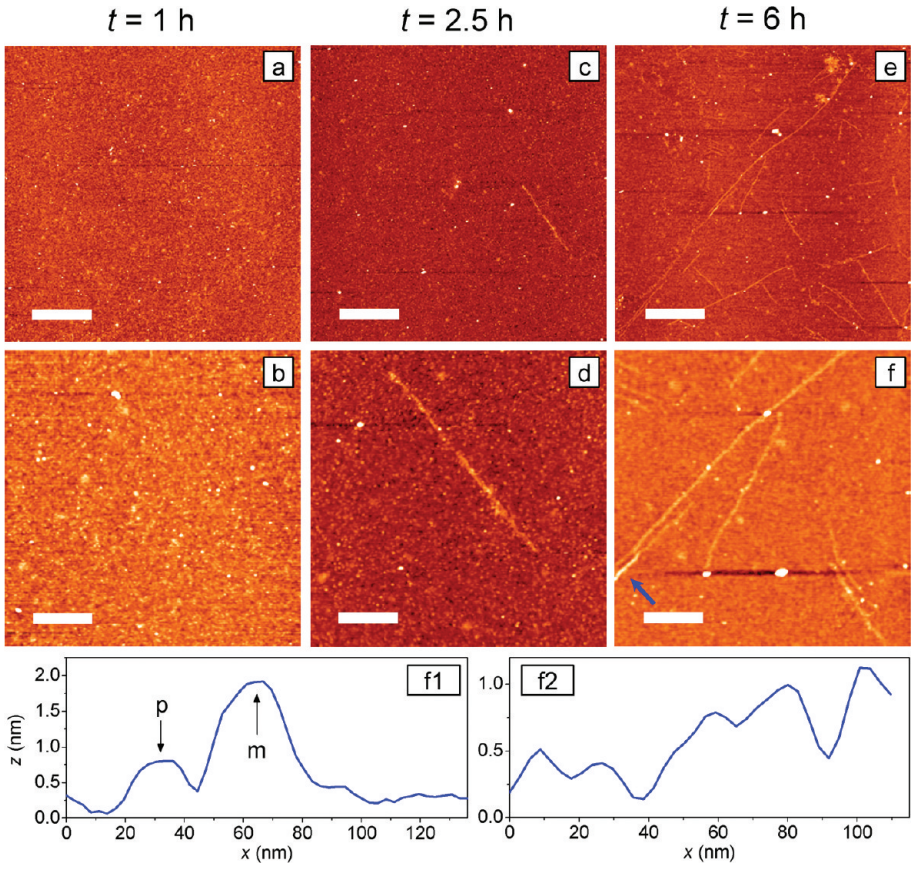

Figure 2. AFM images of the IAPP aggregation on a HC film with $\theta \approx 38°$ at $t = 1$ h (a, b), 2.5 h (c, d), and 6 h (e, f). The scale bars are 660 (upper row) and 220 nm (center row); the height scales are 3 nm (a, b) and 4 nm (c–f). (f1) gives a height profile taken across the proto- (p) and the mature fibril (m) at the position of the arrow in (f). (f2) depicts a height profile taken along the mature fibril.

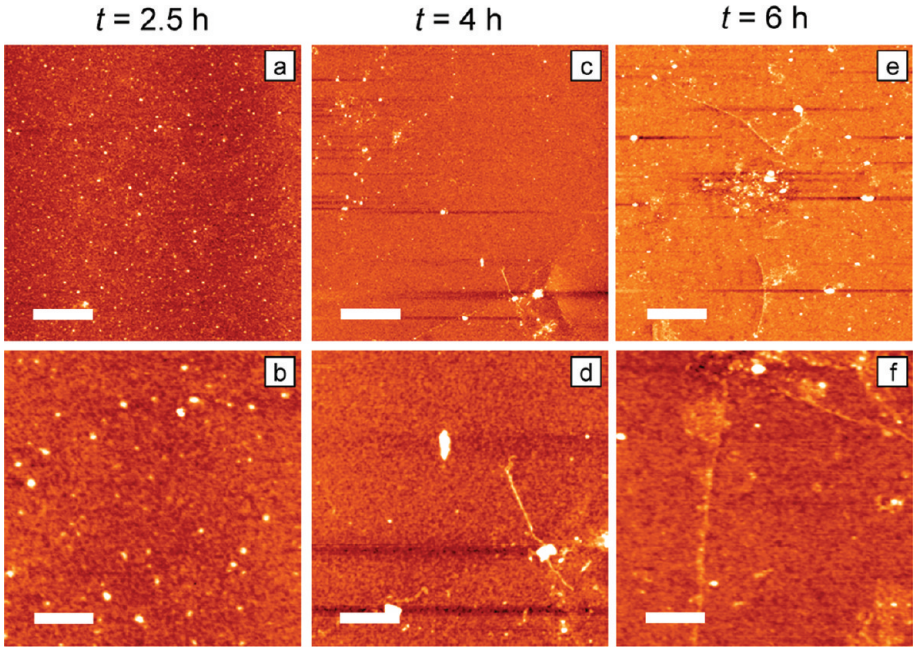

Figure 3. AFM images of the IAPP aggregation on a HC film with $\theta \approx 61°$ at $t = 2.5$ h (a, b), 4 h (c, d), and 6 h (e, f). The scale bars are 660 (upper row) and 220 nm (lower row); the height scales are 3 nm (a–d) and 4 nm (e, f).

amorphous aggregates are the main component of IAPP deposits (see Figure 3e). Moreover, these amorphous aggregates seem to act as seeds for the growth of multiple protofibrils, as can be seen in

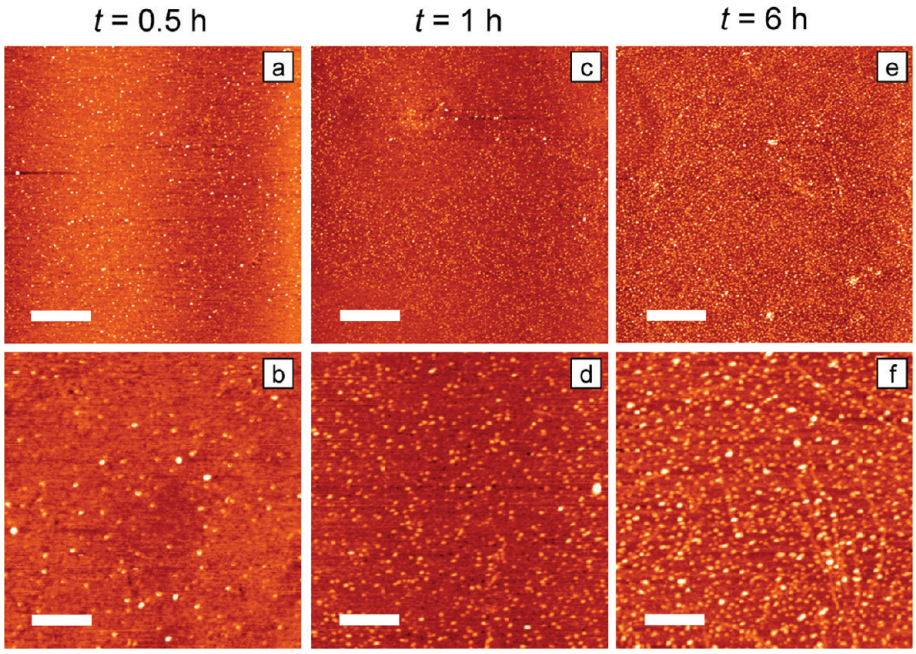

Figure 4. AFM images of the IAPP aggregation on a HC film with $\theta \approx 76°$ at $t = 0.5$ h (a, b), 1 h (c, d), and 6 h (e, f). The scale bars are 660 (upper row) and 220 nm (lower row); the height scales are 2 nm (a–d) and 3 nm (e, f).

Figure 3c–f. This type of fibril growth has already been observed for different amyloid-forming proteins on various surfaces.[9,12,13]

Figure 4 depicts AFM images of the IAPP aggregation on a mica/HC surface with a contact angle of $\theta \approx 76°$. Here, oligomers are again found as the primary species of aggregation from the very beginning (t = 0.5 h, Figure 4a,b). With increasing incubation time, the density of oligomers on the surface increases, but even after 6 h (Figure 4e,f) no closed film has formed. However, at this time some protofibrils are observed between the oligomers in Figure 4f.

For the hydrophobic surface with $\theta \approx 90°$, the IAPP aggregation is again dominated by oligomeric structures. However, the oligomers have a height of 2.6 ± 0.8 nm and are thus significantly larger than in the previous cases. In addition, the aggregation proceeds faster than for $\theta \approx 76°$, as can be seen in Figure 5a,b, which shows a considerably higher density of oligomers after 1 h of incubation compared to Figure 4c,d. After 2.5 h, the oligomer film is almost completely closed (Figure 5c,d). For a further increase of the incubation time, multilayers of oligomers are piling up, resulting in a thick amyloid film, as is depicted in Figure 5e,f.

DISCUSSION

The aggregation of IAPP depends strongly on the hydrophobicity of the surface. Increasing the contact angle of the surface leads to a continuous delay of fibrillation up to a contact angle of 76°. At this angle, protofibrils are just the secondary species and aggregation proceeds primarily *via* oligomeric structures. For the fully hydrophobic surface with $\theta \approx 90°$, no fibrillation is observed within 6 h of incubation, and oligomers represent the only aggregates. The dependence of IAPP aggregation on incubation time t and contact angle θ is summarized in the phase diagram depicted in Figure 6.

Jeworrek *et al*. investigated the adsorption of IAPP on different hydrophilic and hydrophobic polymer surfaces by neutron reflectometry.[22] They found the largest amount of adsorbed IAPP on a hydrophobic polystyrene surface. This finding seems to agree with our observations. After 6 h of incubation, the film adsorbed on the hydrophilic surface ($\theta \approx 23°$) does not cover the whole surface and has a thickness of about 5 nm, corresponding to a monolayer of mature fibrils. In the case of the hydrophobic surface with $\theta \approx 90°$, however, the sample surface seems to be fully covered with several layers of oligomers.

Not only the rate of aggregation but also the structure of the aggregates is influenced by the hydrophobicity of the surface. In the present experiments, fibrillation is observed for hydrophilic surfaces with $\theta \leq 61°$, whereas aggregation of large oligomers dominates on hydrophobic surfaces with $\theta \geq 76°$. In addition, different types of proto- and mature fibrils are found on the hydrophilic surfaces. For the lowest contact angle of $\theta \approx 23°$ the observed protofibrils have a height of 2.0 ± 0.5 nm. This value is in agreement with the protofibril height of 2.4 nm determined for fibrillation of IAPP on freshly cleaved mica surfaces by Goldsbury *et al*.[6] The authors also measured the height and crossover repeat of mature IAPP fibrils. Although their reported crossover repeat of 25 nm is again in fair

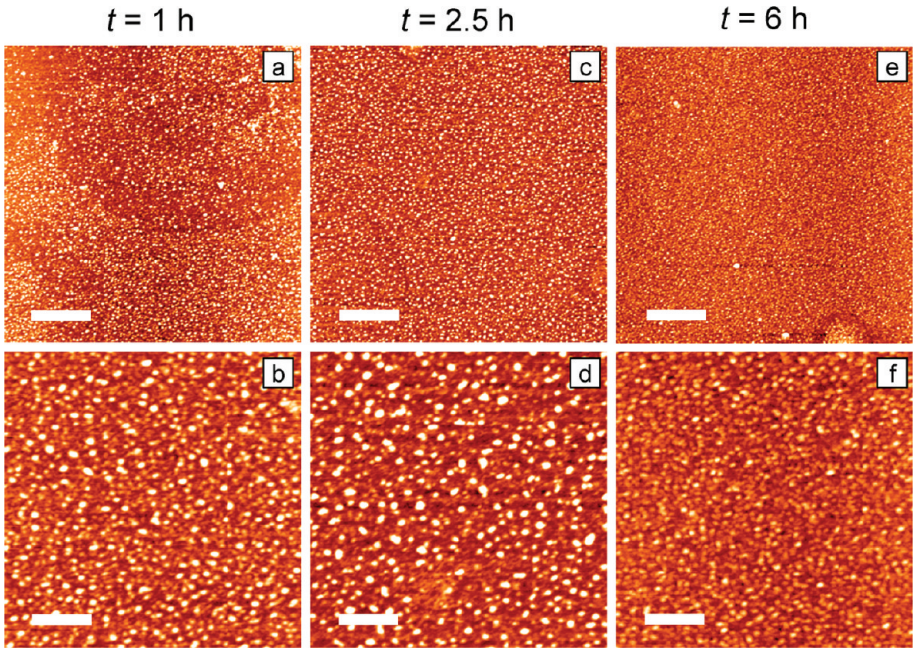

Figure 5. AFM images of the IAPP aggregation on a HC film with $\theta \approx 90°$ at $t = 1$ h (a, b), 2.5 h (c, d), and 6 h (e, f). The scale bars are 660 (upper row) and 220 nm (lower row); the height scale is 4 nm.

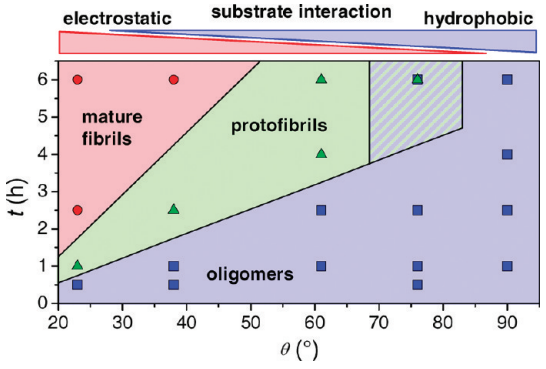

Figure 6. Phase diagram of IAPP aggregation as a function of incubation time t and contact angle θ. The hatched region represents the coexistence of oligomers (primary species) and protofibrils (secondary species). Note that morphological differences between fibrils and oligomers at the different contact angles (see text) are not included.

agreement with the value of 28.4 ± 3.7 nm observed here, they determined the height of the mature fibrils to be 7 nm. This is slightly larger than the value of 4.5 ± 0.5 nm observed in this work. However, since their AFM measurements were performed under liquid conditions, this discrepancy probably results from the dehydration of the fibrils in our experiments. On the more hydrophobic surfaces with $\theta \approx 38°$ and 61°, a different type of protofibril is found that has a smaller height of only 0.9 ± 0.2 nm. The few mature fibrils on the $\theta \approx 38°$ surface consequently also exhibit a reduced height of about 1.8 nm and a crossover repeat of only ~20 nm.

It is widely established that the fibrillar aggregates of IAPP and also other amyloid-forming proteins feature a β-sheet structure.[3,32] In the course of IAPP assembly in the bulk a conformational transition from a random coil to a β-sheet state occurs, whereas the concentration of α-helical structures remains rather constant.[34,35] When interacting with negatively charged lipid interfaces due to electrostatic interactions, however, IAPP was found to adsorb in an α-helical conformation.[17,19] By addition of monomers from the bulk, α-helical aggregates assemble, which then undergo a collective transition to a β-sheet structure and finally form large fibrillar aggregates.[17,19] At the hydrophobic water−air interface on the other hand, only amorphous aggregates were found, although a similar α-helix to β-sheet transition was observed.[19]

At neutral pH, the N-terminal region of IAPP is positively charged, whereas the C-terminal domain is hydrophobic. It is thus reasonable to assume that adsorption of the monomer to negatively charged hydrophilic surfaces occurs through electrostatic interactions with the N-terminus. Adsorption to less charged hydrophobic surfaces on the other hand is presumably dictated by hydrophobic interactions with the C-terminal region. As a consequence, the conformation of the adsorbed monomer is influenced by the type of interaction. Although it is the C-terminal region spanning residues 20−37 that is believed to form the β-sheet structure,[19,36] there are indications that IAPP fibrils are stabilized by both hydrophobic and polar interactions and that also interactions outside the β-sheet core can affect fibril formation.[36] Therefore, different conformations of the initially adsorbed monomers may cause differences in the assembly of the peptides and thus in the molecular structure of the β-sheet aggregates, which in turn can lead to different

types of aggregates, *i.e.*, amorphous aggregates, differently sized oligomers, and fibrils of different morphology. Indeed, a correlation between molecular structure and fibril morphology has been observed for several amyloidogenic molecules[37−39] including the IAPP fragment spanning residues 20−29.[40]

Although AFM yields only topographic information and no structural insight, on the basis of our experiments we can conclude that the type of formed aggregate is dictated by the interplay between hydrophobic and electrostatic interactions with the surface and is very sensitive even to small changes in their relative contributions. Attractive electrostatic interactions with the surface lead to the formation of small oligomers that further assemble to form fibrils, whereas hydrophobic interactions favor aggregates in the form of larger oligomers that are not as prone to fibrillate. At intermediate contact angles around 40°, the electrostatic interactions are less strong and a different type of protofibril with smaller diameter is formed that is likely to consist of even smaller oligomers than the fibrils at more hydrophilic surfaces. At larger contact angles around 60°, the interplay between electrostatic and hydrophobic surface interactions induces the formation of a few large oligomers and amorphous aggregates as the main adsorbate species. The only protofibrils at this contact angle originate from the amorphous aggregates, which act as seeds for fibril growth. At a ∼75° contact angle, where the hydrophobic interactions with the surface are rather strong, oligomers are the primary species of aggregation. Only at high surface coverage are a few protofibrils able to form. At $\theta \approx 90°$, the surface interactions are predominantly hydrophobic and only large oligomers are observed, leading to the fast formation of thick aggregate films.

CONCLUSIONS

In summary, we have shown that the surface hydrophobicity has a strong influence on the surface-catalyzed assembly of IAPP. Increasing the contact angle of a mica/HC surface leads to a continuous and approximately linear increase of the lag time of fibrillation (see Figure 6). The diameter of the formed protofibrils is decreased compared to the case of a lower contact angle of about 20°. At an angle of about 75°, large oligomeric structures become the primary species of aggregation. These observations are attributed to the formation of differently sized oligomers resulting from the interplay between electrostatic and hydrophobic interactions with the surface, which influence the conformation of the initially adsorbed monomers. Electrostatic surface interactions induce the formation of small oligomers that assemble rather fast into fibrils, whereas hydrophobic surface interactions favor the formation of large and more stable oligomers. The relative contributions of these interaction types determine the pathway of aggregation. Our results may contribute to the understanding and control of the surface-catalyzed assembly of disease-related and other peptides. The control of the aggregate type and especially the morphology of amyloid nanofibrils assembled at the surface also has a great potential for technological applications such as the fabrication of biocompatible electrodes for biosensors.[33]

METHODS

The preparation and characterization of the mica/HC samples is described in detail elsewhere.[29] In brief, hyperthermal (<100 eV) Ar ion bombardment of mica leads to the removal of the outermost layer of K^+ ions. Due to an increased number of silicate centers at surface sites, this negatively charged surface exhibits an enhanced reactivity toward HCs, which results in the rapid adsorption of a thin HC film of a few monolayers thickness upon contact with the laboratory atmosphere. When stored under ambient conditions, continuous HC adsorption from the environment leads to a slow increase of the film thickness. In the course of the film growth, the mica/HC surface becomes more hydrophobic, with its contact angle increasing continuously with time until a saturation value of ∼90° is reached after a period of about 3 months. This increase in hydrophobicity is attributed to the interplay between the increased charging of the mica surface and the hydrophobicity of the adsorbed HC film, which partially screens the electric field originating from the charged interface. The chemical composition of the HC films (∼70% of pure HCs and ∼30% of oxygen-containing HCs) does not change during aging and equals the composition of corresponding films adsorbed on nonirradiated mica surfaces.[29] In contrast to other methods that allow the tuning of the hydrophobicity,[41] also the root-mean-square surface roughness of the sample surfaces is almost unaffected by the treatment and ranges from ∼0.5 to ∼1.0 Å. In the current study, ion-beam-modified mica/HC samples with contact angles of 38 ± 3°, 61 ± 1°, 76 ± 2°, and 90 ± 4° have been used, as well as a HC film on an unmodified surface with a contact angle of 23 ± 3°. The surface charge densities (as measured in 3 mM KCl solution) of these samples range from about −10 mC/m^2 for the 23° sample to about −6 mC/m^2 for the 90° sample.[29] The individual samples have been cut into smaller pieces of ∼20 mm^2 to enable several incubations on identical surfaces.

One milligram of synthetic human IAPP(1-37) (American Peptide Company, Inc.) was dissolved in 1 mL of 1,1,1,3,3,3-hexafluoroisopropanol (HFIP, Sigma-Aldrich Co.) at a concentration of 1 mg/mL. The stock was incubated overnight at room temperature and stored at −20 °C prior to use. A 25 μL amount of the HFIP stock was evaporated under vacuum before dissolving in 500 μL of Milli-Q water, yielding a final concentration of 13 μM. After 10 min, 20 μL of the sample was incubated at 25 °C on the mica/HC surfaces in a humidity chamber (humidity >90%). After different time intervals ranging from 0.5 to 6 h, the mica/HC samples were taken out of the humidity chamber and dried over a period of ∼5 min in a stream of nitrogen. In order to avoid any artifacts resulting from possible differences in the sticking of the aggregates to the different hydrophilic and hydrophobic surfaces, the samples were not rinsed before drying. Although this might lead to the deposition of material from the bulk solution, bulk aggregation was found to be only of

minor importance under the present experimental conditions (see Supporting Information for details). In addition, due to the well-controlled incubation conditions, we expect only minor differences between bulk aggregates deposited onto the different sample surfaces. Any observed differences between the individual samples will thus mostly result from the different surface properties. Nevertheless, deposition of monomers from the bulk during the drying cannot be ruled out and may contribute to the formation of the monomer layers observed on the hydrophilic surfaces at short incubation times (see Figure 1).

The dried samples were then imaged by tapping-mode AFM under ambient conditions (25 °C, 34% humidity) using a MultiMode scanning probe microscope with a NanoScope V controller from Veeco Instruments. As has been shown previously, drying does not induce any major changes in the appearance of the IAPP fibrils.[42] In order to minimize the interactions between the AFM tip and the molecules, soft tapping cantilevers with a spring constant of nominally 5 N/m and a tip radius of <10 nm have been used (Tap150Al-G from BudgetSensors).

Acknowledgment. We thank H. Liu and A. Rotaru for help with the sample preparation. We would like to acknowledge financial support from the Danish Basic Research Foundation to the Sino-Danish Center for Molecular Self-assembly, from the Danish Research Councils to the iNANO Center, from the Carlsberg Foundation, from ERC for an advanced grant (F.B.), and from the Alexander von Humboldt foundation (A.K.).

Supporting Information Available: Detailed description of the drying procedure and evaluation of the influence of bulk aggregates. This material is available free of charge *via* the Internet at http://pubs.acs.org.

REFERENCES AND NOTES

1. Sipe, J. D.; Cohen, A. S. History of the Amyloid Fibril. *J. Struct. Biol.* **2000,** *130*, 88–98.
2. Porat, Y.; Kolusheva, S.; Jelinek, R.; Gazit, E. The Human Islet Amyloid Polypeptide Forms Transient Membrane-Active Prefibrillar Assemblies. *Biochemistry* **2003,** *42*, 10971–10977.
3. Höppener, J. W. M.; Ahrén, B.; Lips, C. J. M. Islet Amyloid and Type 2 Diabetes Mellitus. *N. Engl. J. Med.* **2000,** *343*, 411–419.
4. Dong, M. D.; Hovgaard, M. B.; Xu, S.; Otzen, D. E.; Besenbacher, F. AFM Study of Glucagon Fibrillation Via Oligomeric Structures Resulting in Interwoven Fibrils. *Nanotechnology* **2006,** *17*, 4003–4009.
5. Sluzky, V.; Tamada, J. A.; Kilbanov, A. M.; Langer, R. Kinetics of Insulin Aggregation in Aqueous Solutions Upon Agitation in the Presence of Hydrophobic Surfaces. *Proc. Natl. Acad. Sci. U. S. A.* **1991,** *88*, 9377–9381.
6. Goldsbury, C.; Kistler, J.; Aebi, U.; Arvinte, T.; Cooper, G. J. S. Watching Amyloid Fibrils Grow by Time-Lapse Atomic Force Microscopy. *J. Mol. Biol.* **1999,** *285*, 33–39.
7. Kowalewski, T.; Holtzman, D. M. In Situ Atomic Force Microscopy Study of Alzheimer's β-Amyloid Peptide on Different Substrates: New Insights Into Mechanism of β-Sheet Formation. *Proc. Natl. Acad. Sci. U. S. A.* **1999,** *96*, 3688–3693.
8. Blackley, H. K. L.; Sanders, G. H. W.; Davies, M. C.; Roberts, C. J.; Tendler, S. J. B.; Wilkinson, M. J. In-Situ Atomic Force Microscopy Study of β-Amyloid Fibrillization. *J. Mol. Biol.* **2000,** *298*, 833–840.
9. Zhu, M.; Souillac, P. O.; Ionescu-Zanetti, C.; Carter, S. A.; Fink, A. L. Surface-Catalyzed Amyloid Fibril Formation. *J. Biol. Chem.* **2002,** *277*, 50914–50922.
10. Sharp, J. S.; Forrest, J. A.; Jones, R. A. L. Surface Denaturation and Amyloid Fibril Formation of Insulin at Model Lipid-Water Interfaces. *Biochemistry* **2002,** *41*, 15810–15819.
11. Giacomelli, C. E.; Norde, W. Influence of Hydrophobic Teflon Particles on the Structure of Amyloid β-Peptide. *Biomacromolecules* **2003,** *4*, 1719–1726.
12. Hoyer, W.; Cherny, D.; Subramaniam, V.; Jovin, T. M. Rapid Self-Assembly of α-Synuclein Observed by In Situ Atomic Force Microscopy. *J. Mol. Biol.* **2004,** *340*, 127–139.
13. Ban, T.; Hoshino, M.; Takahashi, S.; Hamada, D.; Hasegawa, K.; Naiki, H.; Goto, Y. Direct Observation of Aβ Amyloid Fibril Growth and Inhibition. *J. Mol. Biol.* **2004,** *344*, 757–767.
14. Giacomelli, C. E.; Norde, W. Conformational Changes of the Amyloid β-Peptide (1−40) Adsorbed on Solid Surfaces. *Macromol. Biosci.* **2005,** *5*, 401–407.
15. Rocha, S.; Krastev, R.; Thünemann, A. F.; Carmo Pereira, M.; Möhwald, H.; Brezesinski, G. Adsorption of Amyloid β-Peptide at Polymer Surfaces: A Neutron Reflectivity Study. *ChemPhysChem* **2005,** *137*, 2527–2534.
16. Losic, D.; Martin, L. L.; Aguilar, M.-I.; Small, D. H. β-Amyloid Fibril Formation Is Promoted by Step Edges of Highly Oriented Pyrolytic Graphite. *Biopolymers* **2006,** *84*, 519–526.
17. Knight, J. D.; Hebda, J. A.; Miranker, A. D. Conserved and Cooperative Assembly of Membrane-Bound α-Helical States of Islet Amyloid Polypeptide. *Biochemistry* **2006,** *45*, 9496–9508.
18. Yang, H.; Fung, S.-Y.; Pritzker, M.; Chen, P. Surface-Assisted Assembly of an Ionic-Complementary Peptide: Controllable Growth of Nanofibers. *J. Am. Chem. Soc.* **2007,** *129*, 12200–12210.
19. Lopes, D. H. J.; Meister, A.; Gohlke, A.; Hauser, A.; Blume, A.; Winter, R. Mechanism of Islet Amyloid Polypeptide Fibrillation at Lipid Interfaces Studied by Infrared Reflection Absorption Spectroscopy. *Biophys. J.* **2007,** *93*, 3132–3141.
20. Nayak, A.; Dutta, A. K.; Belfort, G. Surface-Enhanced Nucleation of Insulin Amyloid Fibrillation. *Biochem. Biophys. Res. Commun.* **2008,** *369*, 303–307.
21. Rocha, S.; Thünemann, A. F.; do Carmo Pereira, M.; Coelho, M.; Möhwald, H.; Brezesinski, G. Influence of Fluorinated and Hydrogenated Nanoparticles on the Structure and Fibrillogenesis of Amyloid Beta-Peptide. *Biophys. Chem.* **2008,** *137*, 35–42.
22. Jeworrek, C.; Hollmann, O.; Steitz, R.; Winter, R.; Czeslik, C. Interaction of IAPP and Insulin with Model Interfaces Studied Using Neutron Reflectometry. *Biophys. J.* **2009,** *96*, 1115–1123.
23. Cabaleiro-Lago, C.; Lynch, I.; Dawson, K. A.; Linse, S. Inhibition of IAPP and IAPP$_{(20-29)}$ Fibrillation by Polymeric Nanoparticles. *Langmuir* **2010,** *26*, 3453–3461.
24. Cabaleiro-Lago, C.; Quinlan-Pluck, F.; Lynch, I.; Dawson, K. A.; Linse, S. Dual Effect of Amino Modified Polystyrene Nanoparticles on Amyloid β Protein Fibrillation. *ACS Chem. Neurosci.* **2010,** *1*, 279–287.
25. Mao, X.; Ma, X.; Liu, L.; Niu, L.; Yang, Y.; Wang, C. Structural Characteristics of the Beta-Sheet-Like Human and Rat Islet Amyloid Polypeptides as Determined by Scanning Tunneling Microscopy. *J. Struct. Biol.* **2009,** *167*, 209–215.
26. Mao, X.; Wang, Y.; Liu, L.; Niu, L.; Yang, Y.; Wang, C. Molecular-Level Evidence of the Surface-Induced Transformation of Peptide Structures Revealed by Scanning Tunneling Microscopy. *Langmuir* **2009,** *25*, 8849–8853.
27. Lord, M. S.; Foss, M.; Besenbacher, F. Influence of Nanoscale Surface Topography on Protein Adsorption and Cellular Response. *Nano Today* **2010,** *5*, 66–78.
28. Hlawacek, G.; Puschnig, P.; Frank, P.; Winkler, A.; Ambrosch-Draxl, C.; Teichert, C. Characterization of Step-Edge Barriers in Organic Thin-Film Growth. *Science* **2008,** *321*, 108–111.
29. Keller, A.; Fritzsche, M.; Ogaki, R.; Bald, I.; Facsko, S.; Dong, M. D.; Kingshot, P.; Besenbacher, F. Tuning the Hydrophobicity of Mica Surfaces by Hyperthermal Ar Ion Irradiation. *J. Chem. Phys.* **2011,** *134*, 104705.
30. Anguiano, M.; Nowak, R. J.; Lansbury, P. T. Protofibrillar Islet Amyloid Polypeptide Permeabilizes Synthetic Vesicles by a Pore-like Mechanism that May Be Relevant to Type II Diabetes. *Biochemistry* **2002,** *41*, 11338–11343.
31. Engel, M. F. M.; Khemtémourian, L.; Kleijer, C. C.; Meeldijk, H. J. D.; Jacobs, J.; Verkleij, A. J.; de Kruijff, B.; Killian, J. A.; Höppener, J. W. M. Membrane Damage by Human Islet

Amyloid Polypeptide Through Fibril Growth at the Membrane. *Proc. Natl. Acad. Sci. U. S. A.* **2008,** *105*, 6033–6038.
32. Khemtémourian, L.; Killian, J. A.; Höppener, J. W. M.; Engel, M. F. M. Recent Insights in Islet Amyloid Polypeptide-Induced Membrane Disruption and Its Role in β-Cell Death in Type 2 Diabetes Mellitus. *Exp. Diabetes Res.* **2008,** *2008*, 421287.
33. Gazit, E. Self-Assembled Peptide Nanostructures: the Design of Molecular Building Blocks and Their Technological Utilization. *Chem. Soc. Rev.* **2007,** *36*, 1263–1269.
34. Kayed, R.; Bernhagen, J.; Greenfield, N.; Sweimeh, K.; Brunner, H.; Voelter, W.; Kapurniotu, A. Conformational Transitions of Islet Amyloid Polypeptide (IAPP) in Amyloid Formation in Vitro. *J. Mol. Biol.* **1999,** *287*, 781–796.
35. Goldsbury, C.; Goldie, K.; Pellaud, J.; Seelig, J.; Frey, P.; Müller, S. A.; Kistler, J.; Cooper, G. J. S.; Aebi, U. Amyloid Fibril Formation from Full-Length and Fragments of Amylin. *J. Struct. Biol.* **2000,** *130*, 352–362.
36. Luca, S.; Yau, W.-M.; Leapman, R.; Tycko, R. Peptide Conformation and Supramolecular Organization in Amylin Fibrils: Constraints from Solid-State NMR. *Biochemistry* **2007,** *46*, 13505–13522.
37. Heise, H.; Hoyer, W.; Becker, S.; Andronesi, O. C.; Riedel, D.; Baldus, M. Molecular-Level Secondary Structure, Polymorphism, and Dynamics of Full-Length α-Synuclein Fibrils Studied by Solid-State NMR. *Proc. Natl. Acad. Sci. U. S. A.* **2005,** *102*, 15871–15876.
38. Paravastu, A. K.; Leapman, R. D.; Yau, W.-M.; Tycko, R. Molecular Structural Basis for Polymorphism in Alzheimer's β-Amyloid Fibrils. *Proc. Natl. Acad. Sci. U. S. A.* **2008,** *105*, 18349–18354.
39. Debelouchina, G. T.; Platt, G. W.; Bayro, M. J.; Radford, S. E.; Griffin, R. G Magic Angle Spinning NMR Analysis of β2-Microglobulin Amyloid Fibrils in Two Distinct Morphologies. *J. Am. Chem. Soc.* **2010,** *132*, 10414–10423.
40. Madine, J.; Jack, E.; Stockley, P. G.; Radford, S. E.; Serpell, L. C.; Middleton, D. A. Structural Insights into the Polymorphism of Amyloid-Like Fibrils Formed by Region 20−29 of Amylin Revealed by Solid-State NMR and X-ray Fiber Diffraction. *J. Am. Chem. Soc.* **2008,** *130*, 14990–15001.
41. Zhuang, H.; Song, B.; Srikanth, V. V. S. S.; Jiang, X.; Schönherr, H. Controlled Wettability of Diamond/β-SiC Composite Thin Films for Biosensoric Applications. *J. Phys. Chem. C* **2010,** *114*, 20207–20212.
42. Maurstad, G.; Prass, M.; Serpell, L. C.; Sikorski, P. Dehydration Stability of Amyloid Fibrils Studied by AFM. *Eur. Biophys. J.* **2009,** *38*, 1135–1140.